Indonesian Physical Review
Volume 09 Issue 02, May 2026
P-ISSN: 2615-1278, E-ISSN: 2614-7904

Integrated Satellite Imagery and Geophysical Methods Identify Landslide Susceptibility Zonation in Tabbinjai Village, South Sulawesi

Amirin Kusmiran[1*], Minarti[1], Alvia Auliya[1], Hasmia[1], Wahda Nur Aulia[1], Nisra Azizah[1]
Arif Wijaya[2], Ramadhan Priadi[3]
[1] *Physics Department, Faculty of Science and Technology, Universitas Islam Negeri Alauddin Makassar, Indonesia*
[2] *Mining Engineering, Faculty of Engineering, Muhammadiyah University of Mataram, Mataram, Indonesia*
[3] *Geophysics Station Class II Gowa, Meteorology, Climatology, and Geophysics Agency, Gowa, Indonesia*

Corresponding Author's E-mail: amirin.kusmiran@uin-alauddin.ac.id

Article Info

Article info:
Received: 12-12-2025
Revised: 24-02-2026
Accepted: 26-03-2026

Keywords:
AHP; Integrated Geophysical Methods; Landslide Susceptibility; Satellite Imagery; Tabbinjai Village

How To Cite:
A. Kusmiran, Minarti, A. Auliya, Hasmia, W. N. Aulia, N. Azizah A. Wijaya, R. Priadi "Integrated Satellite Imagery and Geophysical Methods Identify Landslide Susceptibility Zonation in Tabbinjai Village, South Sulawesi", Indonesian Physical Review, vol. 9, no. 2, p 227-247, 2026.

DOI:
https://doi.org/10.29303/ipr.v9i2.632.

Abstract

Tabbinjai Village is susceptible to landslides due to high rainfall, steep topography, and human activities. This study aims to determine the zone of landslide vulnerability using geophysical data and satellite imagery to generate a level of landslide vulnerability map in Tabbinjai Village. The AHP (Analytical Hierarchy Process) method is used to determine the weight composition of satellite imagery data, and Seismic vulnerability and slip plane identification are geophysical methods that include the HVSR (horizontal-to-vertical spectral ratio) method and the Wenner-Schlumberger configuration, respectively. Based on the AHP method, landslide susceptibility is classified into low (60.67%), moderate (37.89%), and high (1.44%) susceptibility zones. These spatial findings are supported by the in situ seismic vulnerability index (Kg) and geoelectrical resistivity profiles, confirming the strong likelihood of slope failure in critical areas. Therefore, integrated satellite imagery and geophysical data provide a reliable reference for regional spatial planning and disaster mitigation strategies.

Introduction

Landslides may be induced by natural and anthropogenic activities. The three types of damage that result from this disaster are environmental, infrastructure, and social. This damage occurred in Tabbinjai Village, Gowa Regency, South Sulawesi [1], [2], [3]. This region is located in an upstream area with very steep topography, high rainfall, and slope instability. It is reported that landslides in Tabbinjai Village damaged roads [1] and affected some residents [2], and this situation required prompt intervention, supported by a detailed landslide susceptibility map, to develop an effective disaster mitigation strategy.

Landslides in Tabbinjai Village are attributed to a combination of governing and triggering factors. Governing factors include lithological and geological structural factors, slope, soil, and land use [4], [5]. In contrast, the triggering factors are usually high rainfall [4], earthquakes, and human activities, such as land use [6], slope cutting [7],[8], and infrastructure development without adequate technical consideration, including slope stability analysis [9]. From a mechanical perspective, the interaction of these factors leads to slope failure when the driving force exceeds the resisting force, causing soil mass to move downslope.

The movement of soil mass is influenced by soil stiffness [10] as indicated by shear wave velocity (Vs). This parameter represents the material's behavior under shear deformation induced by seismic waves. Vs is interpreted using the microtremor method [11], while soil type is interpreted using the geoelectric method [12]. The combination of these methods enables comprehensive site analysis because the microtremor method is sensitive to dynamic response, while the geoelectric method provides the slip plane of the landslide. Soils with lower Vs values deform more readily under dynamic loading. Therefore, the slip plane is prone to landslides caused by impedance contrast between the two layers [11]. The other physical properties extracted from microtremor data are the vulnerability index, dominant frequencies, and amplification factors.

Previous studies have shown that microtremor parameters can be used to identify soft soil and high amplification sites, which are prone to landslides [13], [14], [15]. At the same time, the electrical resistivity method using the Wenner–Schlumberger configuration has also been proven effective for mapping subsurface resistivity variations and detecting the shallow slip surface (weak zone that causes soil movement) [12]. Therefore, the combination of these methods would be a significant contribution to identifying the landslide area at the local scale (as a reference) when integrated with spatial mapping based on satellite imagery.

The necessity for this integration arises from the limitations of satellite approaches. There have been several reports on landslide mapping using remote sensing data [8], [16], [17], but this method cannot capture the influence of soil stiffness on the slip plane. To enhance the accuracy of subsurface landslide susceptibility mapping, this study uses average shear wave velocity to estimate soil stiffness. Soil stiffness and potential slip planes from geophysical methods are used as in situ validation to reduce bias in landslide susceptibility mapping and to provide a more physically consistent representation of slope failure mechanisms.

Therefore, the primary purpose of this study is to identify and map the landslide susceptibility zones in Tabbinjai Village by integrating satellite imagery spatial analysis with in situ geophysical methods (microtremor and geoelectrical resistivity). The results of this comprehensive mapping will be applied to classify landslide susceptibility, providing a reliable reference for government spatial planning and disaster mitigation strategies.

Methodology

Landslide susceptibility mapping

This study adopts a quantitative approach that combines remote sensing and spatial analysis to map land use within a defined Tabbinjai Village region of interest (ROI). Sentinel 2 Level 2A surface reflectance imagery from the COPERNICUS collection on Google Earth Engine (GEE) [18] is used for this purpose, covering the period from 1 January 2025 to 30 September 2025. The image collections are first filtered by date and cloud content using the cloudy percentage attribute (< 15%), then a median composite is created and clipped to the ROI. Land use is mapped using a decision tree method for supervised classification into three main classes (built-up, crop, and vegetation). For land use classification, 80% of the data (553 samples) is used for training, and 20% (138 samples) for testing. Classification performance was assessed using accuracy (≥ 78%) and the Kappa coefficient (Table 1;> 0.76), both of which are acceptable. The final classified map is exported from GEE to Google Drive in the EPSG:4326 coordinate system and limited to the ROI, making it usable for subsequent analysis and visualization in a geographic information system (GIS).

Table 1. Classification of **the** Kappa coefficient ($\mathcal{K}$).

Value of the Kappa coefficient	Nature of agreement
$0.81 \leq \mathcal{K} \leq 1.00$	Almost perfect
$0.61 \leq \mathcal{K} \leq 0.80$	Substantial
$0.41 \leq \mathcal{K} \leq 0.60$	Moderate
$0.21 \leq \mathcal{K} \leq 0.40$	Fair
$0.00 \leq \mathcal{K} \leq 0.20$	Slight
$\mathcal{K} < 0.00$	Poor

The second parameter is a slope map based on Shuttle Radar Topography Mission (SRTM) elevation data at approximately 30 m resolution available from Google Earth Engine. The initial process is to make an ROI for the Tabbinjai Village for slope estimation. The slope values (in degrees) are calculated from the DEM using the Terrain. The slope value categorization, as shown in Table 4, estimates the local inclination for each pixel and exports it from Earth Engine to Google Drive in the EPSG:4326 coordinate system, then clips it to the area of interest, as with all other thematic layers, in standard GIS software. The classification process used six specific parameters; each was scored according to the criteria outlined in Tables 2-7. These parameters served as reference points for categorizing the spatial data, ensuring that the analysis was systematic and reproducible. By quantifying each parameter, this study established a robust framework for evaluating spatial characteristics, supporting more informed decision-making and interpretation based on overlay results. This structured approach enhances the reliability and clarity of the classification outcomes derived from combined spatial datasets.

The third parameter, calculated according to the Rainfall Google Earth Engine script, is an annual rainfall analysis based on the CHIRPS precipitation product. For this layer, annual rainfall from August 2024 to August 2025 is selected by choosing the precipitation band within the CHIRPS. The actual calculation for this layer sums all data within the rainfall accumulation interval, producing a single raster with values for total rainfall (mm/year). The output rainfall data of that calculation is categorized into five categories, as shown in Table 5.

Table 2. Shear wave velocity (V_{S30}) [19].

Class	Interval (m/s)	Score
A	>750	1
B	350-750	2
C	175-350	3
D	< 175	4

Table 3. Distance from road [7].

Class	Interval (m)	Score
High	0-5	4
Moderate	5-10	3
Low	10-20	2
Very low	> 20 m	1

Table 4. Slope [20].

Class	Interval (%)	Score
Very gentle	0–8	1
Gentle	8–15	2
Moderate	15–25	3
Steep	25–45	4
Very steep	>45	5

Table 5. Rainfall intensity [20].

Class	Interval (mm/year)	Score
Very low	<1000	1
Low	1000–2000	2
Moderate	2000–2500	3
High	2500–3000	4
Very high	>3000	5

Table 6. Types of soil [21]**.**

Class	Score
Alluvial, grey alluvial association	1
Mediterranean soil, latosol	2
Brown forest soil	3
Andosol, laterite, grumusol	4
Regosol, lithosol	5

Table 7. Land use [20].

Class	Score
forest/vegetation, water bodies	1
Shrubland	2
Irrigated rice fields	3
Built-up area, crops	4
Bare land	5

The fourth parameter used is proximity analysis to roads, which utilizes road network data from OpenStreetMap (https://www.openstreetmap.org/). Before the analysis is carried out, the road data is ensured to use a projected coordinate system (such as UTM) so that distance units are in meters. The roads are then subjected to concentric buffers around the road segments at 5 m, 10 m, and 20 m in QGIS using the Buffer tool. The buffer results are then reclassified into four proximity classes as shown in Table 3.

To identify the soil type in Tabbinjai Village, we collected data from the FAO digital map (https://www.fao.org/) and classified it according to physical properties that affect infiltration and slope stability (Table 6). The soil stiffness was characterized using VS30 data from the USGS (https://earthquake.usgs.gov/data/vs30/us/). All landslide parameters are converted to the same projection (USGS 84, EPSG 4326) and masked with Tabbinjai Village's administrative boundaries. After that, raster format parameters were converted into vector format before overlay analysis. The criteria for scoring the six parameters in reference to classification are shown in Tables 2-7.

The six parameters above made different contributions to landslide susceptibility (Figure 1), and the size of each parameter's contribution can be expressed by its weight. The parameter weights are calculated using the Analytical Hierarchy Process (AHP) technique. The ranking of the weights is made by prioritizing the landslide controllers through a pairwise comparison method. The pairwise comparison will produce a weighting structure that is more realistic in reflecting their relative importance [20]. The pairwise comparison matrix that represents the realistic arrangement of landslide controllers is assessed using the Consistency Ratio (CR) indicator. If the CR value is less than or equal to 0.1, the weighting structure can be accepted; otherwise, it can be rejected [22]. In this way, landslide susceptibility (LS) can be calculated using Equation 1. Wi and LS are the weight and class score of the *i* th parameter, respectively, according to the classification.

$$LS=\sum_{i=1}^{n}(W_i \times S_i) \quad (1)$$

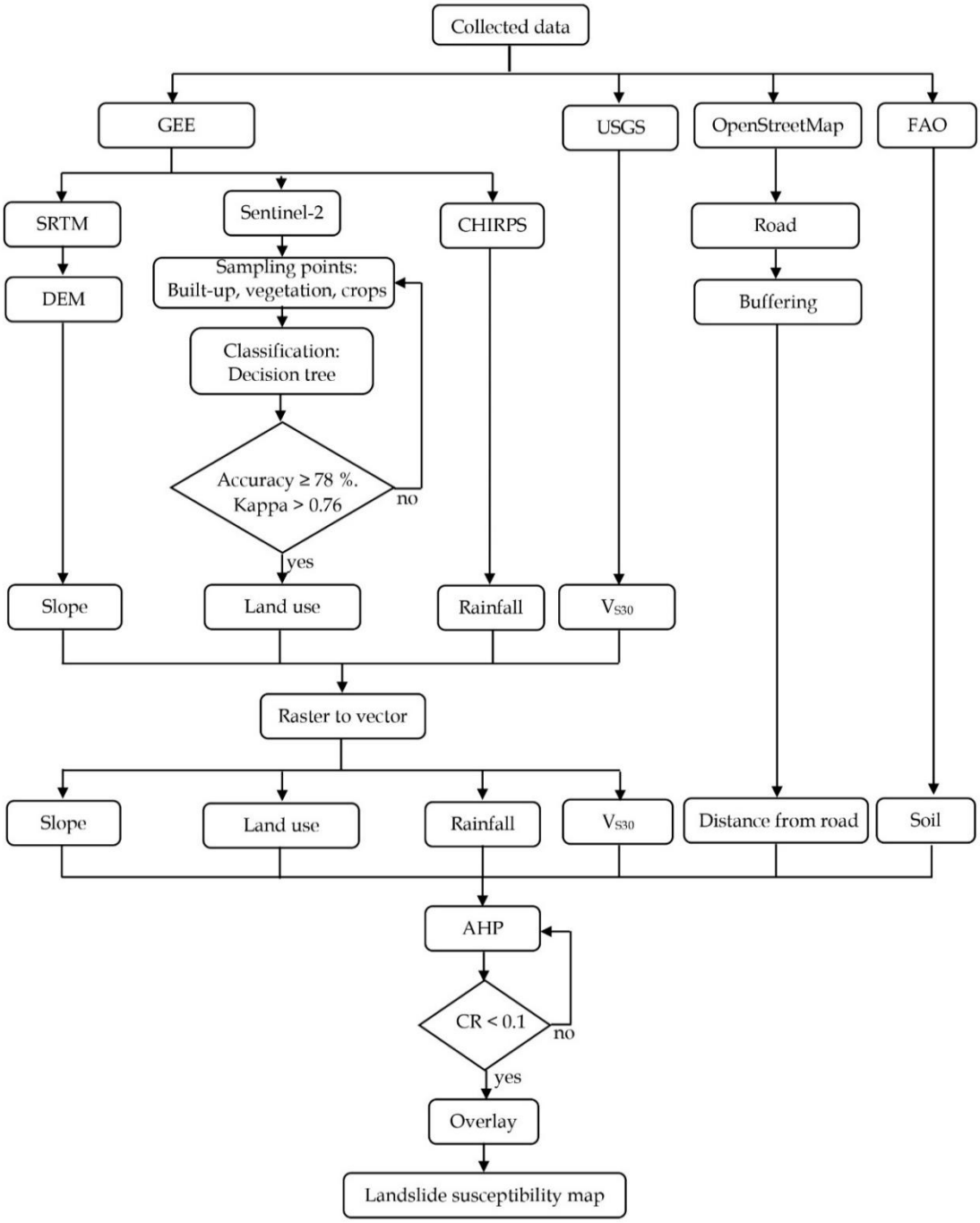

Figure 1. Flowchart of the landslide susceptibility mapping.

Wenner-Schlumberger configuration of geoelectric resistivity

Slip plane and lithology were identified at A_{10} using a Wenner-Schlumberger array. The Wenner-Schlumberger survey used a 100 m profile length with 5 m electrode spacing. The elevation difference between the survey line's start and end points was recorded using GPS. The measurements were conducted using four electrodes (two current and potential electrodes) along the designed survey line, and the measured current and voltage data were used to calculate apparent resistivity. The resistivity cross-section is obtained from inverted apparent resistivity using the Res2Dinv software and can be used to interpret lithology and the slip plane. This interpretation involves matching the measured resistivity with the resistivity ranges for specific rock types and with the local geologic formation of the survey site [23]. The geological formation at the point of measurement is the Qlv formation with rock types of breccia, tuff, lava, and andesite.

Seismic Vulnerability Index (Kg) for Landslide Susceptibility

The purpose of the microtremor data analysis at 14 observation points (Figure 9) was to estimate the surface shear wave velocity distribution. Three-component microtremor recordings with a duration of 1 hour were analyzed using the Geopsy software package [24], [25]. The original signals were bandpass-filtered (0.2–20 Hz) to remove low- and high-frequency noise and windowed. The windowing process is meant to select the windows in time that contain only stationary and stable parts of the signals [26]. Then, the spectra were smoothed using the Konno–Ohmachi method to suppress small-scale fluctuations. The horizontal-to-vertical spectral ratio (HVSR) was calculated for each frequency in the window using Equation 2. HVSR was estimated as the ratio of the combined amplitude spectra of the two horizontal components (North–South and East–West) to the amplitude spectrum of the vertical component.

$$\mathrm{HVSR(f)}=\frac{\sqrt{S_{NS}^2(f)+S_{EW}^2(f)}}{Sv(f)} \quad (2)$$

where $S_{NS}(f)$, S_{EW} (f), and S_V (f) are the Fourier amplitude spectra of North–South, East–West, and vertical components, respectively. In HVSR, the maximum peak gives the dominant frequency F_O and the corresponding amplification factor A_O. These parameters have been used to characterize local site response [27]. The frequency was interpreted using Table 8 to identify lithology, and the amplification classes were determined based on the amplification values in Table 9.

The spectral parameters F_0 and A_0 were subsequently used to derive additional physical parameters, such as the seismic vulnerability index (Kg). This index quantifies the surface soil layer's susceptibility to deformation induced by seismic activity and is computed using Equation 3.

$$K_g=\frac{A_o^2}{F_0} \quad (3)$$

Table 8. Classification of dominant frequencies.

Soil Classification	Frequency dominant (Hz)	Kanai classification	Description
Type I	6.7 - 20.0	Tertiary or older rocks. It consists of hard sandstone, gravel, and other materials.	Surface sediments are very thin in thickness and dominated by hard rock.
Type II	4.0 - 6.7	Alluvial rock with a thickness of 5.0 m. It includes gravel, sand, and hard clay, etc.	The thickness of its surface sediments ranges from 5.0 to 10.0 m.
Type III	2.5 – 4.0	Alluvial rocks with a thickness > 5.0 m. It consists of sandy pebbles, hard clay, and sand, etc.	The surface sediment thickness falls into the medium category of 10–20 meters.
Type IV	< 2.5	Sedimentary rocks are formed by alluvial mud.	The thickness of surface sediments is very thick.

A high Kg value indicates a substantial potential for instability in soft soil layers [24]. The classification of Kg is presented in Table 10.

Table 9. Classification of amplification factor.

Type	Amplification (A_0)	Classification
I	$A_0 < 3$	Low
II	$3 \leq A_0 < 6$	Moderate
III	$6 \leq A_0 < 9$	High
IV	$A_0 \geq 9$	Very high

The shear wave velocity of the first layer, specifically the overburden soil, was determined by inverting the HVSR curve. This procedure was executed using Terrawave software, which employs a global optimization algorithm known as Simulated Annealing.

Table 10. Classification of seismic vulnerability (Kg).

Type	Vulnerability seismic (Kg)	Classification
I	$K_g < 3$	Low
II	$3 \leq K_g < 6$	Moderate
III	$K_g \geq 6$	High

The algorithm operates iteratively to identify a subsurface layer model that produces a synthetic HVSR curve with minimal misfit relative to the field observation curve. Subsequently, all parameters (A_0, K_g, V_S) were spatially mapped using inverse distance weighting (IDW) in QGIS.

Results and Discussion

Land use

The land use distribution in Tabbinjai Village is shown in Figure 2. The classification of Sentinel-2 Satellite Images with an accuracy of 89.52% and a Kappa coefficient of 0.84 provided this information. This spatial arrangement indicates that built-up and crop areas are significantly more exposed to landslide impacts. These findings are consistent with those of Rabby et al. [6] and Hanifuddin et al. [20].

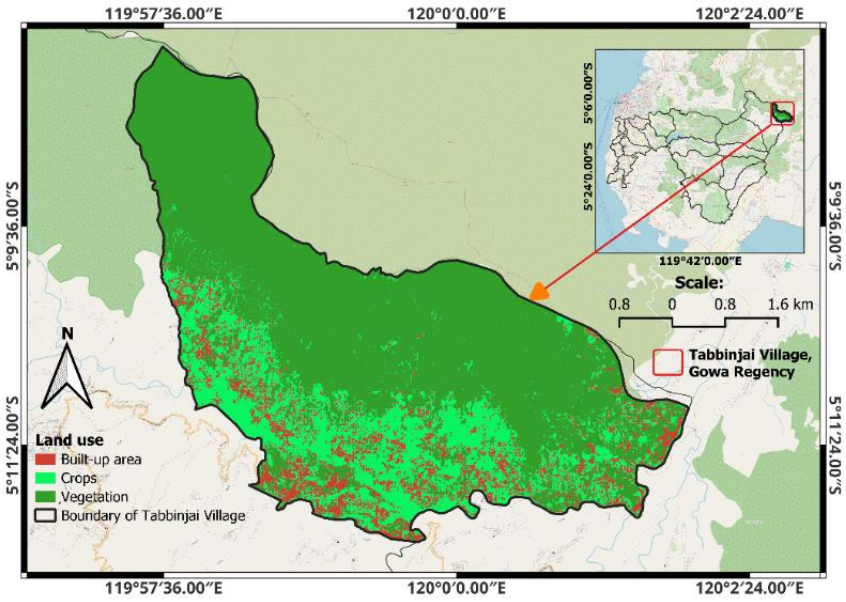

Figure 2. Land use map of Tabbinjai Village.

Both studies support our results, showing that transforming natural vegetation into cultivated lands and built-up areas alters surface hydrology and reduces root cohesion, thereby substantially increasing the region's susceptibility to slope movement. The northern and central parts of the study area are predominantly covered by natural vegetation and crops, which practically occupy the entire area. Therefore, this part still retains a rural image due to its low building density. Urban clusters, residential areas, and associated support infrastructure follow road corridors, with some concentration in the southern part, forming a linear pattern along transportation routes. Cultivated land (crops) is dispersed among settlements and in groups in the central southern zone, indicating a connection between agrarian activities and habitation centers.

Slope

Based on the DEM spatial analysis (Figure 3), the topography of Tabbinjai Village is dominated by steep to very steep slopes. These slopes are predominantly classified as high landslide-susceptibility zones when overlaid with other landslide parameters. These results are aligned with the physical slope stability model described by Shi et al. [25] and Qian et al. [5]. In alignment with their studies, our results indicate that, on such steep inclinations, the gravitational driving forces inherently exceed the soil's internal shear resistance. This unstable condition is further exacerbated in our study area when steep slopes are subjected to external loads, such as water seepage.

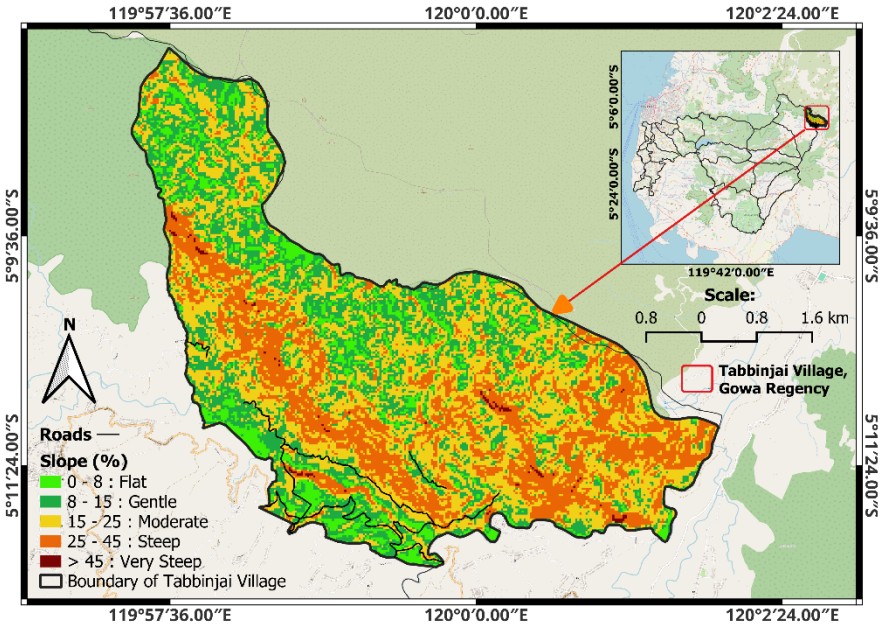

Figure 3. Slope map of Tabbinjai Village.

Rainfall and soil type

Figure 4a represents the mean annual rainfall intensity (mm/year), ranging from 2500 to 3000 mm/year in Tabbinjai Village. The study area is characterized by conditions that strongly contribute to landslide occurrence, as abundant rainfall infiltrates highly porous andosol and regosol soils (Figure 4b). This condition confirms the slope failure mechanisms proposed by Jia et al. [4] and Khan & Wang [28]. Aligning their study, this result shows that intense rainwater infiltration into highly porous topsoil creates a transition zone directly above the bedrock, significantly increasing pore water pressure and reducing effective cohesion, which initiates slope failure and the occurrence of landslides [29], [30].

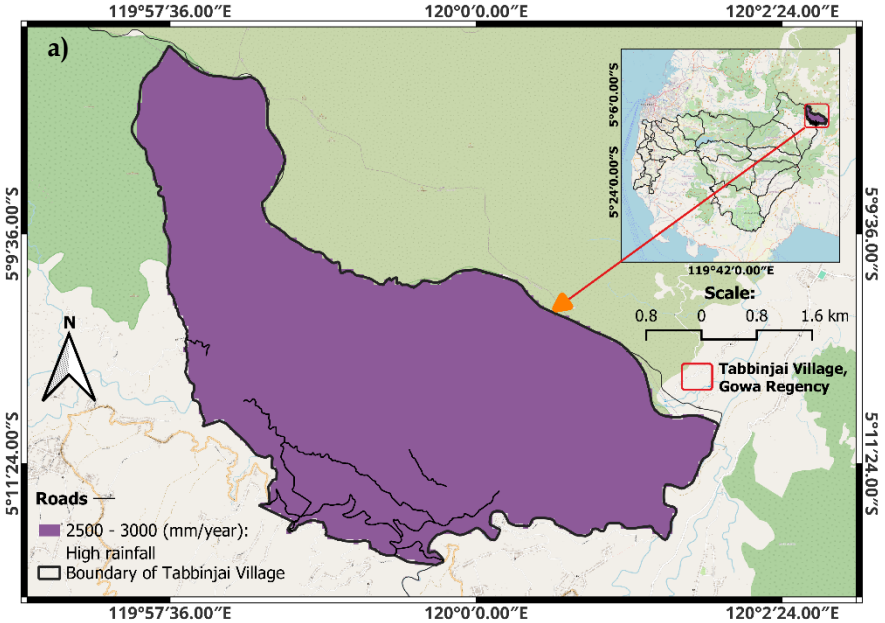

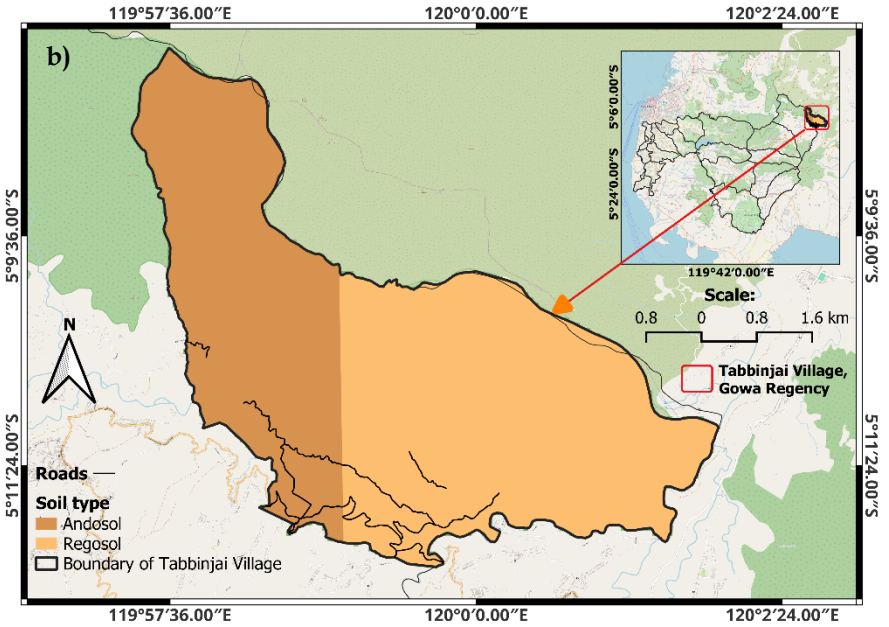

Figure 4. a) Rainfall map, and b) soil type map of Tabbinjai Village.

Distance from Road

The proximity map to roads is shown in Figure 5a. A buffer mapping tool is used to reveal the areas of human activity. Our spatial analysis indicates that the 0-5 m buffer zone directly adjacent to the road networks (the red zone) is most likely to suffer direct damage and exhibits the highest landslide susceptibility. This specific spatial pattern is highly consistent with the research conducted by Pradhan et al. [7] and He et al.[29]. Both of their studies show strong similarities to our findings, demonstrating that artificial steep cuts during road construction physically destroy natural supporting structures and lack adequate drainage, drastically reducing internal resistance during heavy rainfall and triggering instability.

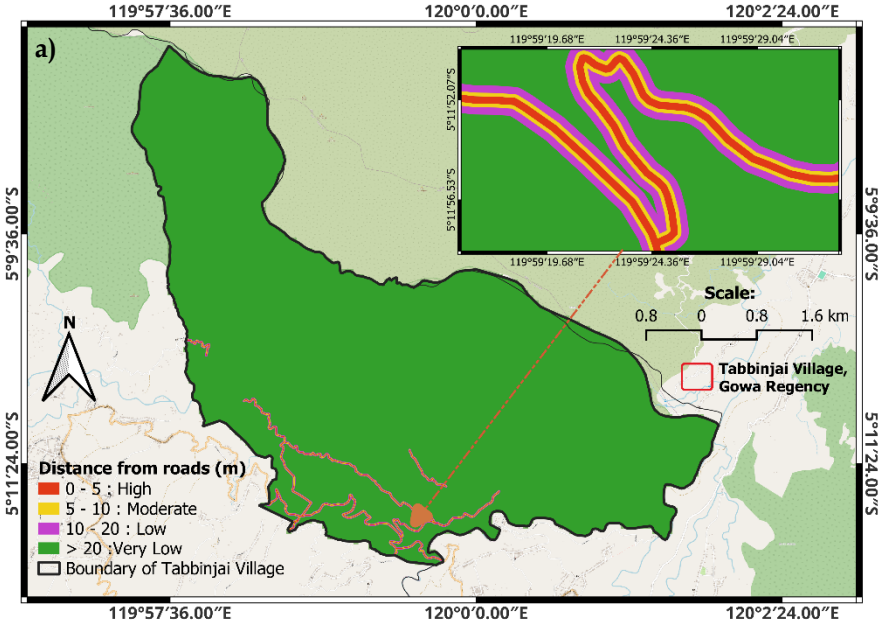

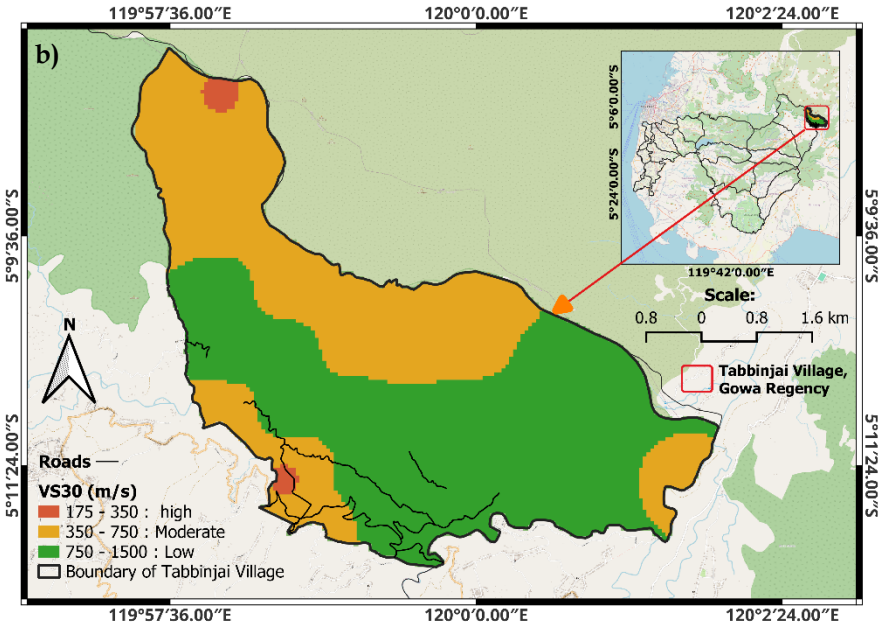

Figure 5. a) Distance from the road map of Tabbinjai Village, and b) V_{S30} map of Tabbinjai Village.

Shaking ground is identified with V_{S30} (Figure 5b). This parameter is used to characterize the stiffness and density of subsurface materials [24]. Variations in velocity values enabled classification of the Tabbinjai Village area into three distinct site-class zones, which were directly associated with slope stability levels.

The central and southern regions were predominantly characterized by green zones with VS30 values ranging from 750 to 1500 m/s, so this zone was classified as site class A (i.e., rock) based on Table 2 and had low landslide susceptibility. Conversely, the northern region and a small section in the southwest (orange zones) exhibit V_{S30} values of 350–750 m/s. This result corresponds to site class B (very dense soil and soft rock), so this zone was classified as moderate susceptibility. Zones with high susceptibility are indicated by red areas (such as the northernmost and southwestern regions) with V_{S30} values of 175–350 m/s. These areas are associated with site class C (stiff/medium soils). Low shear wave velocity indicates less consolidated materials that are prone to deformation or mass movement during slope instability. Once all the variables were identified. Furthermore, the next step involved integrating geophysical parameters with the surface characteristic data.

Landslide susceptibility

Six parameters related to landslide control and triggering (rainfall intensity, slope, land use, soil, distance from road, and VS30) are spatially combined to map landslide susceptibility (Figure 6). A weight-of-map-overlay approach for this mapping is calculated using the AHP method. The weights of each parameter (Table 11) are 0.4060 for rainfall, 0.2560 for slope, 0.1150 for V_{S30}, 0.0909 for distance from road, 0.0590 for land use, and 0.0340 for soil. The weight is CR compliant as this product satisfies the requirements of CR with a value of 0.080 or lower.

Table 11. Calculation of landslide susceptibility.

No.	Parameter	Score (Si)	Wi	Wi × Si
1	Rainfall	4	0.4060	1.6240
2	Slope	1		0.2560
		2		0.5120
		3	0.2560	0.7680
		4		1.0240
		5		1.2800
3	V_{S30}	2		0.2300
		3	0.1150	0.3450
		4		0.4600
4	Distance from road	1		0.0909
		2	0.0909	0.1818
		3		0.2727
		4		0.3636
5	Land use	1	0.0590	0.0590
		4		0.2360
6	Soil type	4	0.0340	0.1360
		5		0.1700
Total amount of LS max				**4.1136**

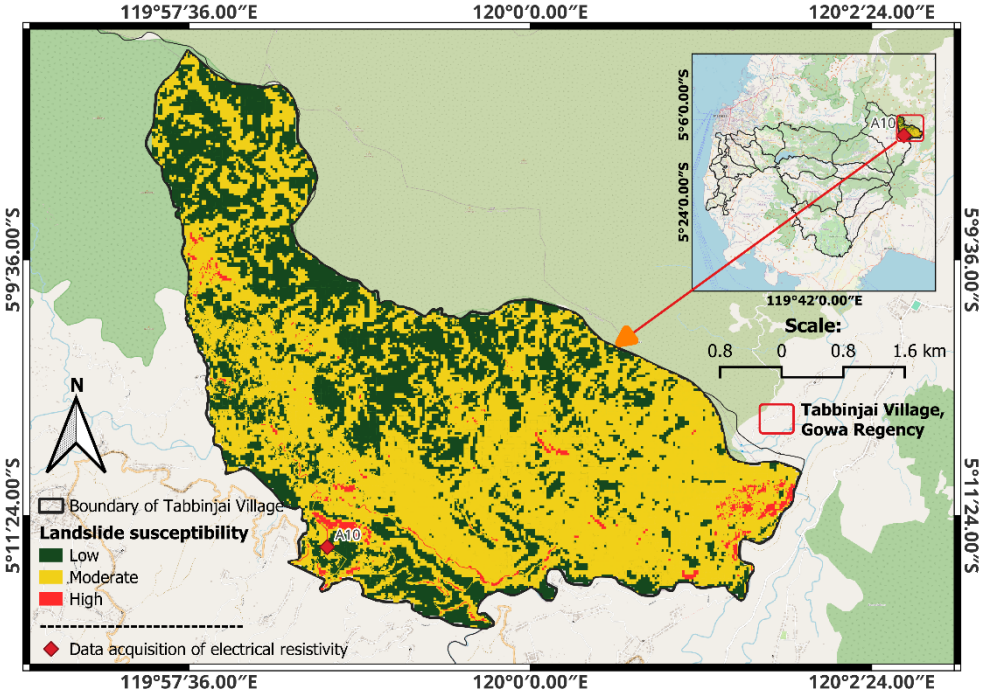

Figure 6. Landslide susceptibility in Tabbinjai Village.

The study area in Figure 6 is categorized into three landslide susceptibility zones: low, moderate, and high. As detailed in Table 12, the area study is predominantly characterized by low (60.67%) and moderate (37.89%) susceptibility, with only 1.44% at high risk. The high susceptibility zone (red) shows a spatial pattern that extends along the road network in Tabbinjai Village in the southern region and forms a significant cluster in the western area.

Table 12. Landslide susceptibility area.

No.	Landslide susceptibility	Area (ha)	Area (%)
1	High	35.03	1.44
2	Moderate	922.74	37.89
3	Low	1477.63	60.67
Total		**2435.41**	**100**

This pattern indicates that dominant factors, such as road construction and slope excavation, markedly increase landslide occurrence. Meanwhile, the cluster of red zones in the west is highly correlated with physical geological conditions, including Andosol soil layers with low V_{S30} values (Type C). One of the anthropogenic parameters in the 0–5 m road buffer zone has made this area the most critical due to the loss of slope support after construction activities. This result is consistent with the findings of Jia et al. [4] and Khan & Wang [28] who showed that anthropogenic modification can increase landslide susceptibility. On the other hand, the low-susceptibility zones (green) that dominate the northern and eastern regions are characterized by natural slope stability and dense forest vegetation. Furthermore, the yellow transition zone (moderate susceptibility) generally occupies mixed agricultural areas with moderate hazard potential but requires vigilance during periods of extreme rainfall. In addition, the susceptibility of this zone may increase if land use is not properly controlled, particularly due to deforestation. These spatial correlations align with the landslide assessments conducted by Rabby et al. [6] and Hanifuddin et al. [20], confirming that dense natural vegetation effectively preserves slope stability and minimizes landslide susceptibility.

Wenner-Schlumberger configuration of geoelectric resistivity

The geoelectrical resistivity survey line is located in the Southwestern high susceptibility area at the A10 point (Figure 6) and on the Qlv geological formation. The resistivity values obtained from the geoelectric inversion of the Wenner-Schlumberger configuration are between 4.41 and 326 Ωm (Figure 7). Based on geological formation (Qlv), the first layer (15.1 to 326 Ωm) is interpreted as regosol/andosols. The high resistivity of this layer is attributed to very dry surface conditions and to solid layers (highlighted in yellow), such as a breccia layer outcropping on the surface.

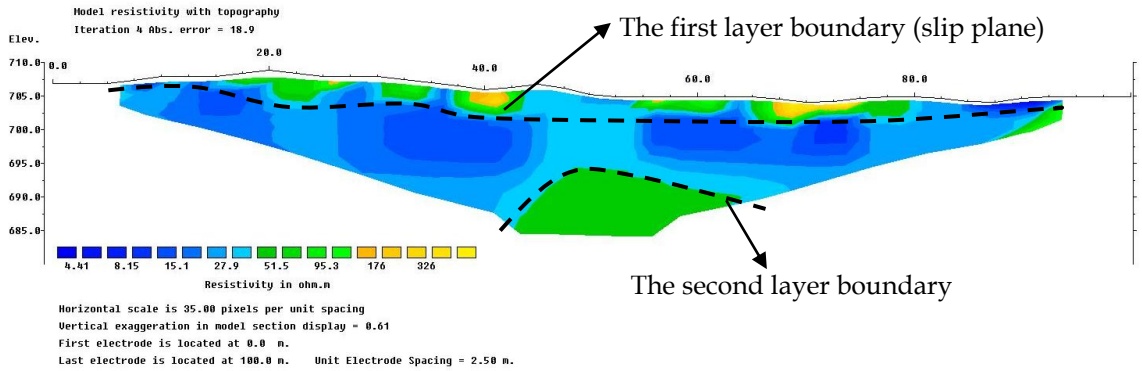

Figure 7. Cross-section of Wenner–Schlumberger configuration.

The resistivity of the second layer ranges from 4.41 to 27.9 Ωm. This resistivity range was interpreted as tuff. The tough layer exhibits low resistivity, indicating that it is water-saturated (or infiltrated). The contact between the tuff and the regosol/andosol in Figure 7,

located at a depth of approximately 3 meters, is considered a probable slip plane. This resistivity contrast aligns with the geophysical findings reported by Tsai et al. [12] and represents a weak zone that likely initiates slope instability and triggers landslides.

Furthermore, the third layer had a resistivity value of 95.3 Ωm, and was interpreted as a breccia. This breccia layer also has a relatively low value due to extensive infiltration, which may lead to weathering. This geoelectric cross-section was used as a constraint in the 1D HVSR inversion of the microtremor data.

Seismic Vulnerability Index (Kg) for Landslide Susceptibility

The subsurface has been investigated using the HVSR method at 14 measurement sites shown in Figure 9a, with sample HVSR curves shown in Figure 8. The results show variations in the dominant frequency (F_0) and amplification factor (A_0), suggesting that the study area has heterogeneous subsurface layers. The dominant frequencies (2.71 to 10.8 Hz) reflected the variation in the thickness of the surface sediment layer (the cover layer). High dominant frequency values (F_0 > 6.7 Hz) at points A_5 (10.8 Hz) and A_4 (9.64 Hz) are interpreted as shallow volcanic rock or very thin soil. On the other hand, low dominant frequencies (F_0 < 4.0 Hz) at points A_7, A_{10}, and A_{13} (Table 13) are interpreted as thick and soft sediment layers that are lithologically related to eroded volcanic soil (andosol/regosol). These results are related to studies by Setiawan et al. [31] and Molnar et al. [32], which confirms that low dominant frequencies are directly associated with thick deposits of unconsolidated, soft volcanic soils.

The A_0 in Figure 9b has values from 2.4 to 7.69. These values are interpreted as seismic wave amplification due to impedance contrast between soft soil layers and bedrock. The highest amplification is observed at points A_{13} (A_0 = 7.69) and A_7 (A_0 = 5.39). The high amplification values in this area indicate a significant density contrast, resulting in lower density and shear wave velocity than bedrock. This condition enhances the potential hazard of wave shaking, as soft soil layers tend to amplify the energy of propagating vibrations [32], [33].

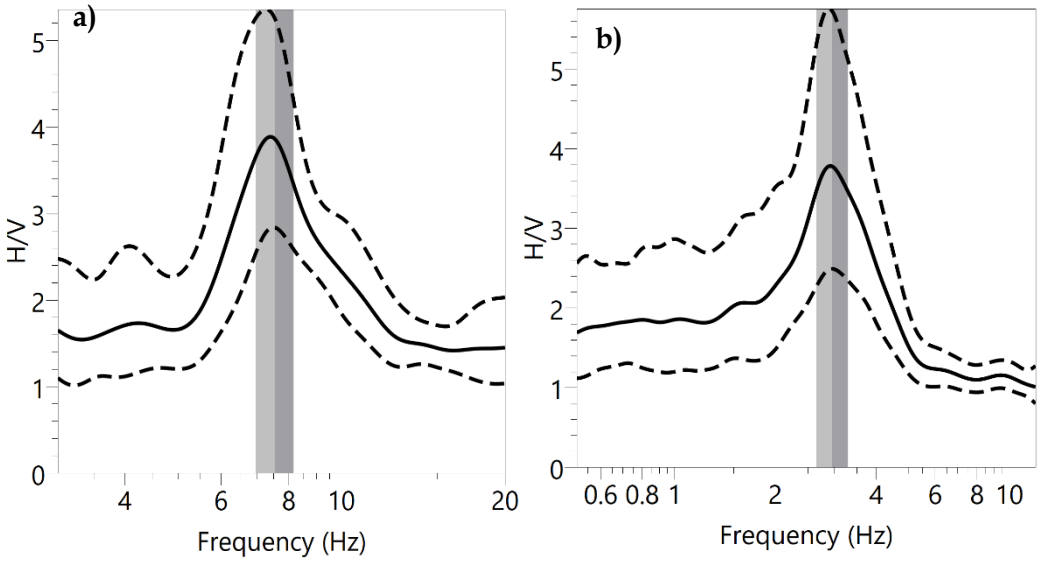

Figure 8. HVSR curve of a) acquisition at site (point) 11, and b) acquisition at site (point) 12.

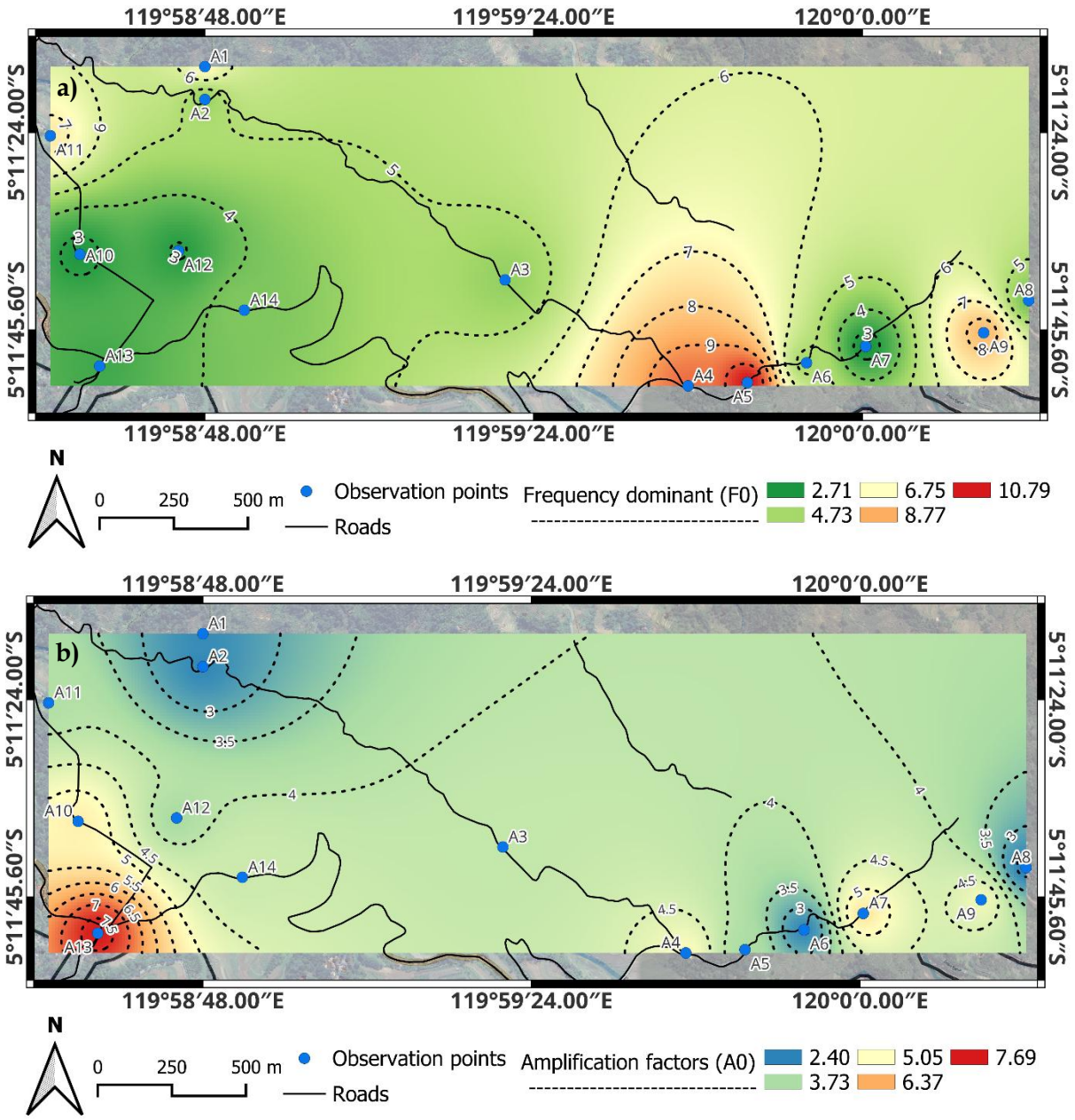

Figure 9. a) Dominant frequency map, and b) Amplification factor map.

The seismic vulnerability shown in Figure 10 was used to map the soil deformation zone as a susceptible area. The Kg values range from 0.95 to 17.97. These values are interpreted to indicate that the area studied has low to high landslide susceptibility. High seismic vulnerability index values were identified at points A_{13} (Kg = 17.97), A_7 (Kg = 10.72), and A_{10} (Kg = 9.92). These high Kg values indicate that the soil layers at these points are very unstable and highly susceptible to plastic deformation when saturated [32]. Spatial correlation indicates that points with higher Kg values are located in landslide-prone areas. One of the values in the area between the road slope cutting is A_7. This result confirms that soft soil and anthropogenic interventions are the most important variables controlling slope instability in Tabbinjai Village.

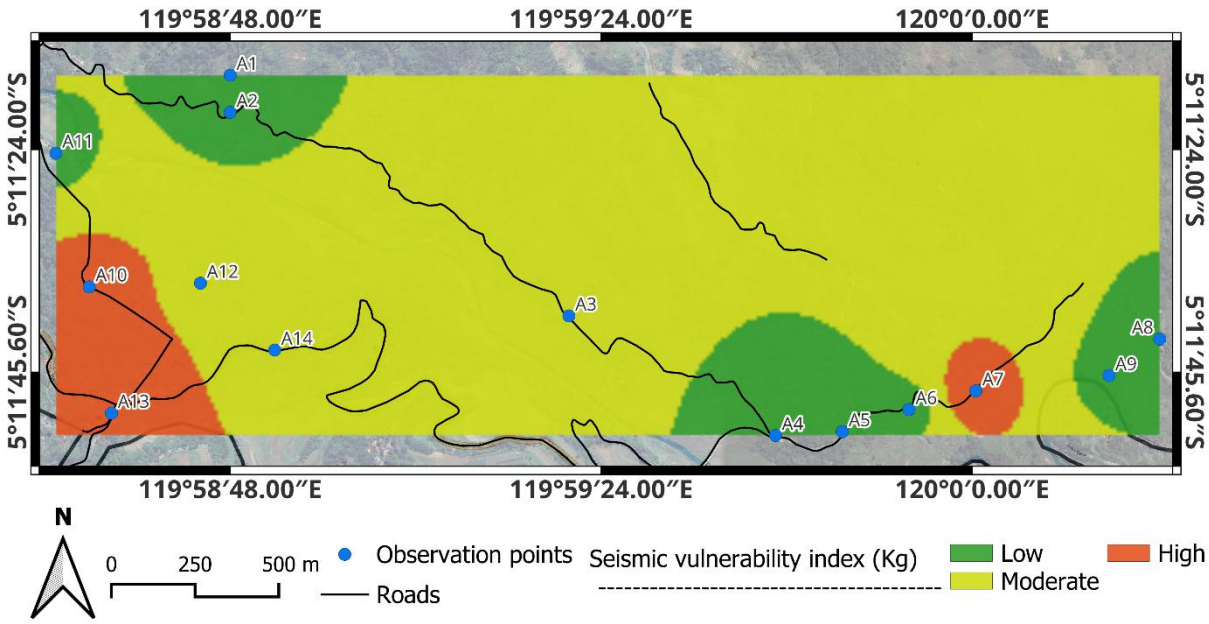

Figure 10. Seismic vulnerability index map.

Correlation between landslide susceptibility and seismic vulnerability index

We inverted the HVSR curve to obtain a 1D V_S profile for interpreting soil stiffness. The V_S distribution map of the first layer in Figure 11a shows a range of shear wave velocities from 150 to 500 m/s, and low values (blue-green) indicate soft sediments, and high values (yellow-orange) are present for stiffer layers. When correlated with the seismic vulnerability index (Figure 11b), zones with relatively low VS values are classified as having moderate to high landslide susceptibility (yellow and red). Meanwhile, areas with higher Vs values are generally associated with low landslide susceptibility (green). This spatial correspondence indicates that the soft, shallow layers tend to amplify shock amplitudes that increase the seismic vulnerability index, which implies a high potential for damage and slope instability [4], [31].

The high seismic vulnerability at A_7, A_{10}, and A_{13} sites has V_S that varies between 150 and 300 m/s (blue) (Table 13). Based on SNI 1726:2019 [19], these velocity values indicate very dense soil and soft rock (Type C), which are dominated by topsoil with a coarse texture, such as andosols or regosol, resulting from volcanic weathering. The low V_S under the top layer is the dominant factor driving slope instability in Tabbinjai Village. In soil mechanics, VS values below 300 m/s are consistent with low shear modulus and high porosity. On the other hand, sites with V_S values exceeding 400 m/s (orange) are interpreted as stable or low in landslide susceptibility.

The landslide susceptibility map was validated using the seismic vulnerability index (Figure 11b). This figure compares the spatial landslide susceptibility map with in situ geophysical properties. High seismic vulnerability index values were identified at point A_7, A_{10}, and A_{13} (Table 13). These values indicate unstable soil layers that are highly susceptible to deformation when saturated.

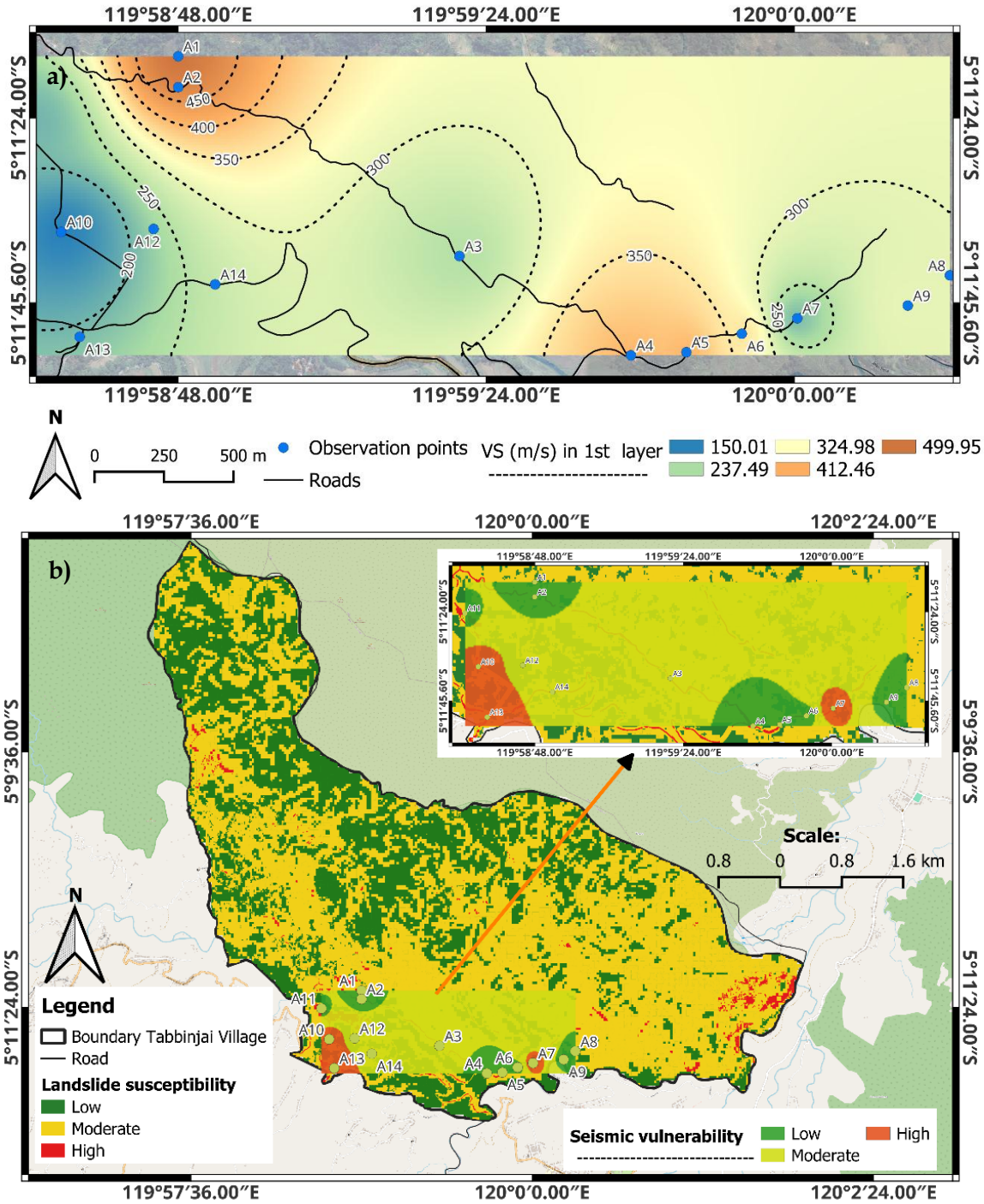

Figure 11. a) Shear wave velocity of the first layer (Vs), and b) Landslide susceptibility with seismic vulnerability index map overlay.

The seismic vulnerability index is high in this susceptibility zone, suggesting that it may have eroded soil layers with strong vibration amplification and a high sensitivity to plastic deformation when saturated with water. Furthermore, the road network is highly susceptible to landslides. These findings demonstrate the influence of human factors on slope

stability. This observation is also evident at point A_{10}, which is located in an area characterized by a high Kg value, low V_S, and moderate landslide susceptibility (Table 13).

Table 13. Landslide susceptibility and physical properties of each site (point).

Site	F_O (Hz)	A_O	V_S (m/s)	Kg	LS
A1	6.72	2.53	500	Low	Moderate
A2	4.6	2.5	250	Low	Low
A3	4.51	4.12	400	Moderate	Moderate
A4	9.64	4.97	400	Low	High
A5	10.8	3.8	350	Low	High
A6	4.81	2.51	210	Low	Moderate
A7	2.71	5.39	300	High	Moderate
A8	4.17	2.4	150	Low	Moderate
A9	8.4	4.82	200	Low	Low
A10	2.81	5.28	150	High	Moderate
A11	7.23	3.86	160	Low	High
A12	2.96	3.76	230	Moderate	Low
A13	3.29	7.69	210	High	High
A14	4.21	4.26	280	Moderate	Moderate

This low-velocity anomaly coincides with the shallow slip plane previously identified in the geoelectrical cross section (Figure 7), confirming that the structural weakness initiates at this depth. These findings agree with the high Kg. Moreover, the low-susceptibility zone in the north of the study area is positively associated with low Kg values (A_1, A_2, and A_5 sites). This relationship typically indicates good slope stability in volcanic rocks near the surface. Therefore, it can be concluded that the correspondence between the regional landslide susceptibility model and in situ geophysical parameters is acceptable for describing the zoning map of potential sliding in Tabbinjai Village. Integrating macroscale satellite imagery with microscale geophysical validation significantly reduces uncertainty, enabling the spatial model of landslide susceptibility to serve as a robust basis for disaster mitigation strategies. Furthermore, it provides a critical scientific basis for formulating safe spatial planning and infrastructure development policies, particularly for enforcing strict engineering standards for road excavations and drainage systems within the identified high susceptibility zones [7], [29].

Conclusion

The landslide susceptibility map of Tabbinjai Village was classified into three landslide susceptibility zones: low (60.67%), moderate (37.89%), and high (1.44%). The high landslide susceptibility zone in the South and West is due to anthropogenic perturbation and the low shear wave velocity of the first layer. These results were validated using the seismic vulnerability index. The landslide susceptibility map can be used for disaster mitigation and land-use planning in Tabbinjai Village, Gowa Regency. A limitation of this study is the absence of direct geotechnical drilling to validate the precise soil shear strength. Therefore, additional research may include soil mechanics testing to calibrate soil shear strength parameter values.

References

[1] S. Z. S. Wahab and H. Latif, "Akses Jalan Desa Tabbinjai Gowa Sulsel Tak Bisa Dilalui Imbas Longsor," Tribun-timur.com. Accessed: Dec. 30, 2025. [Online]. Available: https://makassar.tribunnews.com/2024/07/03/akses-jalan-desa-tabbinjai-gowa-sulsel-tak-bisa-dilalui-imbas-longsor

[2] A. A. F. N. Irfan, "2 Rumah di Gowa Rusak Diterjang Longsor Imbas Hujan Lebat Sepekan," Detiksulsel. Accessed: Dec. 30, 2025. [Online]. Available: https://www.detik.com/sulsel/berita/d-7421503/2-rumah-di-gowa-rusak-diterjang-longsor-imbas-hujan-lebat-sepekan

[3] Kementerian Kesehatan Republik Indonesia, "Tanah Longsor di GOWA, Sulawesi Selatan, 25-04-2020." Accessed: Dec. 30, 2025. [Online]. Available: https://pusatkrisis.kemkes.go.id/Tanah-Longsor-di-GOWA-SULAWESI-SELATAN-25-04-2020-14

[4] Y. Jia, S. Luan, M. Saleh Asheghabadi, D. Xing, H. Yuan, and J. Liu, "Slope stability analysis of coastal geotechnical structures under combined effects of earthquake and rainfall," *Frontiers in Earth Science*, vol. 11, Jan. 2024.

[5] Z.-H. Qian, J.-F. Zou, and Q.-J. Pan, "3D Discretized Rotational Failure Mechanism for Slope Stability Analysis," Nov. 2021, Accessed: Dec. 30, 2025. [Online]. Available: https://ascelibrary.org/doi/10.1061/%28ASCE%29GM.1943-5622.0002163

[6] C. Dai, W. Li, H. Lu, and S. Zhang, "Landslide Hazard Assessment Method Considering the Deformation Factor: A Case Study of Zhouqu, Gansu Province, Northwest China," *Remote Sensing*, vol. 15, p. 596, Jan. 2023.

[7] X. Chen *et al.*, "Conv-trans dual network for landslide detection of multi-channel optical remote sensing images," *Frontiers in Earth Science*, vol. 11, p. 1182145, May 2023.

[8] J. Li *et al.*, "Assessing the soil moisture effects of planted vegetation on slope stability in shallow landslide-prone areas," *Journal of Soils and Sediments*, vol. 21, no. 7, pp. 2551–2565, Apr. 2021.

[9] Y. W. Rabby, Y. Li, J. Abedin, and S. Sabrina, "Impact of Land Use/Land Cover Change on Landslide Susceptibility in Rangamati Municipality of Rangamati District, Bangladesh," *ISPRS International Journal of Geo-Information*, vol. 11, no. 2, p. 89, Jan. 2022.

[10] S. Pradhan, D. Toll, N. Rosser, and M. Brain, "An investigation of the combined effect of rainfall and road cut on landsliding," *Engineering Geology*, vol. 307, p. 106787, July 2022.

[11] A. Pyakurel, D. K. C., and B. K. Dahal, "Enhancing co-seismic landslide susceptibility, building exposure, and risk analysis through machine learning," *Scientific Reports*, vol. 14, no. 1, p. 5902, Mar. 2024.

[12] W.-N. Tsai et al., "Electrical Resistivity Tomography (ERT) Monitoring for Landslides: Case Study in the Lantai Area, Yilan Taiping Mountain, Northeast Taiwan," Front. Earth Sci., vol. 9, pp. 1–19, Oct. 2021.

[13] M. Oleng, Z. Ozdemir, and K. Pilakoutas, "Co-seismic and rainfall-triggered landslide hazard susceptibility assessment for Uganda derived using fuzzy logic and geospatial modelling techniques," *Natural Hazards*, vol. 120, no. 15, pp. 14049–14082, July 2024.

[14] Z. Xu, A. Che, and H. Zhou, "Seismic landslide susceptibility assessment using principal component analysis and support vector machine," *Scientific Reports*, vol. 14, no. 1, p. 3734, Feb. 2024.

[15] H. Shu, Z. Guo, S. Qi, D. Song, H. R. Pourghasemi, and J. Ma, "Integrating Landslide Typology with Weighted Frequency Ratio Model for Landslide Susceptibility Mapping: A Case Study from Lanzhou City of Northwestern China," *Remote Sensing*, vol. 13, no. 18, p. 3623, Sept. 2021.

[16] H. Albanwan, R. Qin, and J.-K. Liu, "Remote Sensing-Based 3D Assessment of Landslides: A Review of the Data, Methods, and Applications," *Remote Sensing*, vol. 16, no. 3, p. 455, Jan. 2024.

[17] N. Zhou, J. Hong, W. Cui, S. Wu, and Z. Zhang, "A Multiscale Attention Segment Network-Based Semantic Segmentation Model for Landslide Remote Sensing Images," *Remote Sensing*, vol. 16, no. 10, p. 1712, May 2024.

[18] I. H. Y. Kwong, F. K. K. Wong, and T. Fung, "Automatic Mapping and Monitoring of Marine Water Quality Parameters in Hong Kong Using Sentinel-2 Image Time-Series and Google Earth Engine Cloud Computing," Front. Mar. Sci., vol. 9, pp. 1–18, May 2022.

[19] BSN, *SNI 1726:2019: Tata Cara Perencanaan Ketahanan Gempa untuk Struktur Bangunan Gedung dan Nongedung*. Badan Standar Nasional, 2019.

[20] F. Hanifudin, A. L. Nugraha, and H. S. Firdaus, "Analisis Pengaruh Perubahan Tutupan Lahan Terhadap Ancaman Bencana Longsor Dengan Menggunakan Sistem Informasi Geografis (Studi Kasus: Kabupaten Kebumen)," *Jurnal Geosains dan Teknologi*, vol. 7, no. 1, pp. 36–46, Oct. 2024.

[21] H. Setiawan and A. Wibowo, "Analysis Of Landslide Susceptibility In The Cugenang New Fault Area In The North Of Cianjur Regency," *Jurnal Geografi Edukasi dan Lingkungan (JGEL)*, vol. 7, pp. 94–108, July 2023.

[22] B. Zhang, W. Pedrycz, A. R. Fayek, and Y. Dong, "A Differential Evolution-Based Consistency Improvement Method in AHP With an Optimal Allocation of Information Granularity," *IEEE Transactions on Cybernetics*, vol. 52, no. 7, pp. 6733–6744, July 2022.

[23] E. D. Ebong, A. Agwul, E. Bekongshelhe, and L. Ebong, "Geoelectrical Resistivity and Geological Characterization of Hydrostructures for Groundwater Resource Appraisal in the Obudu Plateau, Southeastern Nigeria," *Natural Resources Research*, vol. 30, Feb. 2021.

[24] A. I. Hadi *et al.*, "Zonation of Seismic Vulnerability Levels in South Bengkulu Regency, Indonesia for Disaster-Based Regional Planning," *Rudarsko-geološko-naftni zbornik*, vol. 39, no. 2, pp. 133–148, Apr. 2024.

[25] X. Shi, J. Wang, M. Jiang, S. Zhang, Y. Wu, and Y. Zhong, "Extreme rainfall-related accelerations in landslides in Danba County, Sichuan Province, as detected by InSAR," *International Journal of Applied Earth Observation and Geoinformation*, vol. 115, p. 103109, Dec. 2022.

[26] D.-J. Jwo, W.-Y. Chang, and I.-H. Wu, "Windowing Techniques, the Welch Method for Improvement of Power Spectrum Estimation," *Computers, Materials & Continua*, vol. 67, pp. 3983–4003, Jan. 2021.

[27] G. Zhou and H. Yao, "Shallow Structure and Seismic Amplification Effects in the Weifang Segment of the Tanlu Fault Zone Based on the Spectral Ratio Method," *Seismological Research Letters*, vol. 96, Aug. 2024.

[28] M. I. Khan and S. Wang, "Slope Stability Analysis to Correlate Shear Strength with Slope Angle and Shear Stress by Considering Saturated and Unsaturated Seismic Conditions," *Applied Sciences*, vol. 11, no. 10, p. 4568, May 2021.

[29] H. He, X. Dong, S. Du, H. Guo, Y. Yan, and G. Chen, "Study on the Stability of Cut Slopes Caused by Rural Housing Construction in Red Bed Areas: A Case Study of Wanyuan City, China," *Sustainability*, vol. 16, no. 3, p. 1344, Feb. 2024.

[30] A. Solgi, E. Zenner, R. Naghdi, M. Ali, R. Shoja, and F. Behjou, "Evaluating the Effectiveness of Mulching for Reducing Soil Erosion in Skid Trail Switchbacks," *Croatian journal of Forest Engineering*, vol. 43, June 2022.

[31] S. Molnar *et al.*, "A review of the microtremor horizontal-to-vertical spectral ratio (MHVSR) method," *Journal of Seismology*, vol. 26, no. 4, pp. 653–685, Mar. 2022.

[32] C. P. Ramos, N. A. Abrahamson, and R. Kayen, "Estimation of site terms in ground-motion models for California using horizontal-to-vertical spectral ratios from microtremor", Accessed: Dec. 30, 2025. [Online]. Available: https://pubs.usgs.gov/publication/70237838

[33] D. Setiawan, N. Haerudin, B. Sapto, M. Sarkowi, and S. Erfani, "Identification of Landslide-Prone Areas Using the Horizontal to Vertical Spectral Ratio (HVSR) Method and the GIS Approach in Semakai District, Tanggamus Regency, Lampung Province," *Jurnal Fisika Flux: Jurnal Ilmiah Fisika FMIPA Universitas Lambung Mangkurat*, vol. 20, p. 154, July 2023.